Inorganic Chemistry
Article

Inorg. Chem. **2009,** *48,* 4997–5004 **4997**
DOI:10.1021/ic900059m

Ni(II)/H_2O_2 Reactivity in Bis[(pyridin-2-yl)methyl]amine Tridentate Ligand System. Aromatic Hydroxylation Reaction by Bis(μ-oxo)dinickel(III) Complex

Atsushi Kunishita,[‡] Yoshitaka Doi,[‡] Minoru Kubo,[§] Takashi Ogura,[§] Hideki Sugimoto,[‡] and Shinobu Itoh*[,†,∥]

[†]*Department of Material and Life Science, Division of Advanced Science and Biotechnology, Graduate School of Engineering, Osaka University, 2-1 Yamada-oka, Suita, Osaka 565-0871, Japan,* [‡]*Department of Chemistry, Graduate School of Science, Osaka City University, 3-3-138 Sugimoto, Sumiyoshi-ku, Osaka 558-8585, Japan,* [§]*Research Institute of Picobiology, Graduate School of Life Science, University of Hyogo, 3-2-1 Kouto, Kamigori-cho, Ako-gun, Hyogo 678-1297, Japan, and* [∥]*Institute for Molecular Science, National Institutes of Natural Sciences, 38 Nishigo-Naka, Myodaiji, Okazaki 444-8585, Japan*

Received January 13, 2009

The nickel(II) complexes $\mathbf{1^X}$ supported by bis[(pyridin-2-yl)methyl]benzylamine tridentate ligands carrying *m*-substituted phenyl groups (X = OMe, Me, H, Cl, NO_2) at the 6-position of pyridine donor groups (L^X, *N,N*-bis[(6-*m*-substituted-phenylpyridin-2-yl)methyl]benzylamine) have been synthesized and characterized. The X-ray crystallographic analyses have revealed that $[Ni^{II}(L^H)(CH_3CN)(H_2O)](ClO_4)_2$ ($\mathbf{1^H}$), $[Ni^{II}(L^{OMe})(CH_3CN)(MeOH)](ClO_4)_2$ ($\mathbf{1^{OMe}}$), $[Ni^{II}(L^{Me})(CH_3CN)(H_2O)](ClO_4)_2$ ($\mathbf{1^{Me}}$), and $[Ni^{II}(L^{Cl})(CH_3CN)(H_2O)](ClO_4)_2$ ($\mathbf{1^{Cl}}$) have a five-coordinate square pyramidal geometry, whereas $[Ni^{II}(L^{NO_2})(CH_3CN)_2(H_2O)](ClO_4)_2$ ($\mathbf{1^{NO_2}}$) exhibits a six-coordinate octahedral geometry having an additional CH_3CN co-ligand. ^1H NMR spectra of the nickel(II) complexes $\mathbf{1^X}$ in CD_3CN have indicated that all the complexes have a high spin ground state. The nickel(II) complexes $\mathbf{1^X}$ react with hydrogen peroxide (H_2O_2) in acetone to give bis(μ-oxo)dinickel(III) complexes $\mathbf{2^X}$ exhibiting a characteristic UV−vis absorption band at ∼420 nm. In the case of $\mathbf{2^H}$, a resonance Raman band ascribable to a Ni_2O_2 core vibration was observed at 611 cm^{-1} that shifted to 586 cm^{-1} upon $H_2{}^{18}O_2$. The bis(μ-oxo)dinickel(III) intermediates $\mathbf{2^X}$ undergo an efficient aromatic ligand hydroxylation reaction, producing a mononuclear nickel(II)-phenolate complexes $\mathbf{4^X}$ via a putative intermediate (μ-phenoxo)(μ-hydroxo)dinickel(II) ($\mathbf{3^X}$). The kinetic studies on the aromatic ligand hydroxylation process including *m*-substituent effects (Hammett analysis) and kinetic deuterium isotope effects (KIE) have indicated that the reaction of $\mathbf{2^X}$ to $\mathbf{3^X}$ involves an electrophilic aromatic substitution mechanism, where C−O bond formation and C−H bond cleavage occur in a concerted manner. Intermediate $\mathbf{3^H}$ was detected by ESI-MS during the course of the reaction, and the final product $\mathbf{4^H}$ was characterized by elemental analysis, ESI−MS, and X-ray crystallographic analysis.

Introduction

Nickel/active-oxygen complexes have attracted much recent attention because of their relevance to the dioxygen activation mechanism by transition metal complexes. So far, bis(μ-oxo)dinickel(III) complex **A**, bis(μ-1,2-superoxo)dinickel(II) complex **B**, mononuclear (η^2-superoxo)nickel(II) complex **C**, and (*tert*-butylperoxo)nickel(II) complex **D** have been structurally characterized by X-ray crystallographic analysis, and their physicochemical properties have been explored in detail.[1−4] Formation of (μ-1,2-peroxo)dinickel-(II) complex **E** as well as (η^1-superoxo)nickel(II) complex **F** has also been demonstrated in some ligand systems.[5,6]

*To whom correspondence should be addressed. E-mail: shinobu@msl.eng.osaka-u.ac.jp.

(1) (a) Hikichi, S.; Yoshizawa, M.; Sasakura, Y.; Akita, M.; Moro-oka, Y. *J. Am. Chem. Soc.* **1998**, *120*, 10567–10568. (b) Itoh, S.; Bandoh, H.; Nagatomo, S.; Kitagawa, T.; Fukuzumi, S. *J. Am. Chem. Soc.* **1999**, *121*, 8945–8946. (c) Shiren, K.; Ogo, S.; Fujinami, S.; Hayashi, H.; Suzuki, M.; Uehara, A.; Watanabe, Y.; Moro-oka, Y. *J. Am. Chem. Soc.* **2000**, *122*, 254–262. (d) Mandimutsira, B. S.; Yamarik, J. L.; Brunold, T. C.; Gu, W.; Cramer, S. P.; Riordan, C. G. *J. Am. Chem. Soc.* **2001**, *123*, 9194–9195. (e) Itoh, S.; Bandoh, H.; Nakagawa, M.; Nagatomo, S.; Kitagawa, T.; Karolin, K. D.; Fukuzumi, S. *J. Am. Chem. Soc.* **2001**, *123*, 11168–11178. (f) Schenker, R.; Mandimutsira, B. S.; Riordan, C. G.; Brunold, T. C. *J. Am. Chem. Soc.* **2002**, *124*, 13842–13855.

(2) (a) Yao, S.; Bill, E.; Milsmann, C.; Wieghardt, K.; Driess, M. *Angew. Chem., Int. Ed.* **2008**, *47*, 7110–7113. (b) Otsuka, S.; Nakamura, A.; Tatsuno, Y. *J. Am. Chem. Soc.* **1969**, *91*, 6994–6999.

(3) Fujita, K.; Schenker, R.; Gu, W.; Brunold, T. C.; Cramer, S. P.; Riordan, C. G. *Inorg. Chem.* **2004**, *43*, 3324–3326.

(4) Hikichi, S.; Okuda, H.; Ohzu, Y.; Akita, M. *Angew. Chem., Int. Ed.* **2009**, *48*, 118–191.

(5) (a) Kiber-Emmons, M. T.; Schenker, R.; Yap, G. P. A.; Brunold, T. C.; Riordan, C. G. *Angew Chem., Int. Ed.* **2004**, *43*, 6716–6718. (b) Schenker, R.; Kiber-Emmons, M. T.; Riordan, C. G.; Brunold, T. C. *Inorg. Chem.* **2005**, *44*, 1752–1762.

(6) Kiber-Emmons, M. T.; Annaraj, J.; Seo, M. S.; Heuvelen, K. M. V.; Tosha, T.; Kitagawa, T.; Brunold, T. C.; Nam, W.; Riordan, C. G. *J. Am. Chem. Soc.* **2006**, *128*, 14230–14231.

Published on Web 4/17/2009

Scheme 1

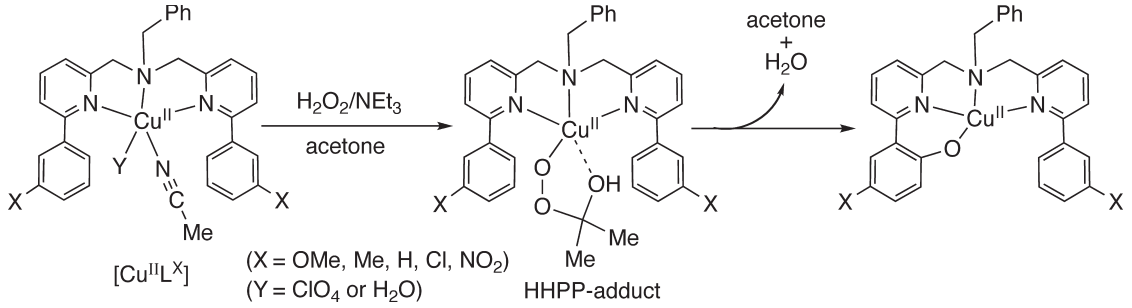

With respect to the reactivity of the nickel/active-oxygen complexes, aliphatic ligand hydroxylation reaction in **A** has been examined most extensively to explore that the reaction involves a hydrogen atom abstraction and oxygen rebound mechanism.[1b,1e] Oxygen atom transfer reaction from **C**, **E**, and **F** to PPh_3 has also been examined briefly.[3,5,6] The structure and reactivity of these nickel/active-oxygen complexes have frequently been discussed in connection with those of the related copper/active-oxygen complexes.[7]

As a part of our continuing research on dioxygen activation chemistry by copper complexes, we have recently examined H_2O_2-reactivity of the copper(II) complexes $Cu^{II}L^X$ supported by the bis[(pyridin-2-yl)methyl]benzylamine tridentate ligands carrying *m*-substituted 6-phenyl groups on the pyridine donor groups (L^X) to find the formation of a unique 2-hydroxy-2-hydroperoxypropane (HHPP) adduct in acetone (Scheme 1).[8,9] From this HHPP-adduct, an aromatic ligand hydroxylation reaction took place effectively to give a copper(II)-phenolate complex via an electrophilic aromatic substitution mechanism (Scheme 1), providing an important insight into the oxygenation ability of the mononuclear copper(II)-peroxo species.[8,9]

In this study, we have extended our research to the nickel(II) system using the same ligand L^X to evaluate the reactivity difference between the nickel(II) and the copper(II) complexes. In the nickel system as well, a similar aromatic ligand hydroxylation reaction took place to give a nickel(II)-phenolate complex $\mathbf{4^X}$. However, the reactive intermediate in this reaction was found to be a bis(*μ*-oxo)dinickel(III) complex, but not a HHPP-adduct of Ni(II). Thus, the results will provide further insight into the oxygen activation chemistry by transition metal complexes.

Experimental Section

General Information. The reagents and the solvents used in this study, except the ligands and the nickel complexes, were commercial products of the highest available purity and were further purified by the standard methods, if necessary.[10] *N,N*-bis[(6-*p*-substituted-phenylpyridin-2-yl)methyl]benzylamine ligands (L^X) were prepared by the reported methods.[11] FT-IR spectra were recorded on a Jasco FTIR-4100, and UV−visible spectra were taken on a Hewlett-Packard 8453 photo diode array spectrophotometer equipped with a Unisoku thermostatted cell holder USP-203. ^{1}H NMR spectra were recorded on a JEOL FT-NMR GX-400 spectrometer or a Bruker AVANCE 600 spectrometer. 2D NOESY spectra were obtained in a phase-sensitive mode using the pulse sequence 90° - t_1 - 90° - Δ_m - 90° and using TPPI method. The optimum mixing times Δ_m cover the range 0.6−0.8 s. Other parameter settings were as follows: SW = 10080.65 Hz in both dimensions, 2 K data block (f_2), 4 scans, and 48 dummy scans in 1024 increments (f_1). 1D NOESY spectra were obtained in a phase-sensitive mode using selective refocusing with a shaped pulse. The parameter settings were as follows: SW = 9615.38 Hz spectral width, 64 K data points with a 350 ms shaped pulse named Gause1.1000 by the Bruker standard version and a 3.41 s acquisition time. In this method, measuring transient NOE enhancements which, by the use of pulse field gradients, avoids the need to compute difference spectra and thus give spectra which contain no subtraction artifacts. As a result, very small NOE enhancements can be detected readily and with much confidence. In all measurements TMS was used as an internal reference. Mass spectra were recorded on a JEOL JMS-700T Tandem MS-station mass spectrometer. Resonance Raman scattering was excited at 406.7 nm from Kr^+ laser (Spectra Physics, BeamLok 2060). Resonance Raman scattering was dispersed by a single polychromator (Ritsu Oyo Kogaku, MC-100) and was detected by a liquid nitrogen cooled CCD detector (Roper Scientific, LNCCD-1100-PB). The resonance Raman measurements were carried out using a rotated cylindrical cell thermostatted at −80 °C or a rotating NMR tube (outer diameter = 5 mm) thermostatted at −90 °C by flashing cold nitrogen gas. A 135° backscattering geometry was used. Elemental analyses were recorded with a Perkin-Elmer or a Fisons instruments EA1108 Elemental Analyzer.

Chart 1

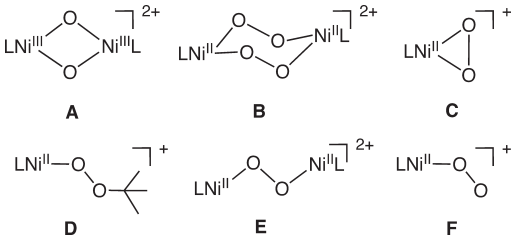

Synthesis of Nickel(II) Complexes. *Caution! The perchlorate salts in this study are all potentially explosive and should be handled with care.*

$[Ni^{II}(L^H)(CH_3CN)(H_2O)](ClO_4)_2$ (1^H). $Ni^{II}(ClO_4)_2 \cdot 6H_2O$ (145.6 mg, 0.40 mmol) was added to a CH_3CN-CH_3OH (1:1) solution (5 mL) of ligand L^H (176.4 mg, 0.40 mmol). After stirring for 10 min at room temperature, insoluble material was removed by filtration. Addition of ether (100 mL) to the filtrate gave blue powder that was precipitated by standing the mixture for several minutes. The supernatant was then removed by decantation, and the remaining blue solid was washed with

(7) Suzuki, M. *Acc. Chem. Res.* **2007**, *40*, 609–617.
(8) Kunishita, A.; Teraoka, J.; Scanlon, J. D.; Matsumoto, T.; Suzuki, M.; Cramer, C. J.; Itoh, S. *J. Am. Chem. Soc.* **2007**, *129*, 7248–7249.
(9) Kunishita, A.; Scanlon, J. D.; Ishimaru, H.; Honda, K.; Ogura, M.; Suzuki, M.; Cramer, C. J.; Itoh, S. *Inorg. Chem.* **2008**, *47*, 8222–8232.
(10) Armarego, W. L. F.; Perrin, D. D. In *Purification of Laborator Chemicals*, 4th ed.; Butterworth-Heinemann: Oxford, 1996; pp 176, 215.
(11) Kunishita, A.; Osako, T.; Tachi, Y.; Teraoka, J.; Itoh, S. *Bull. Chem. Soc. Jpn.* **2006**, *79*, 1729–1741.

ether three times and dried to give complex $\mathbf{1^H}$ in 88%. FT-IR (KBr) 3416 cm^{-1} (OH), 1124, 1054, and 626 cm^{-1} (ClO_4^-); HR-MS (FAB, pos.) m/z = 499.1549 calcd for $C_{31}H_{27}N_3Ni$: 499.1558; Anal. Calcd for $[Ni^{II}(L^H)(CH_3CN)(H_2O)](ClO_4)_2$ ($C_{33}H_{32}NiCl_2N_4O_9$): C, 52.27; H, 4.25; N, 7.39. Found: C, 52.02; H, 4.21; N, 7.28.

$[Ni^{II}(L^{OMe})(CH_3CN)(MeOH)](ClO_4)_2$($1^{OMe}$). This compound was synthesized in a similar manner using ligand L^{OMe} (100.2 mg, 0.2 mmol) instead of L^H as green powder in 77%. FT-IR (KBr) 3358 cm^{-1} (OH), 1254 cm^{-1}(OMe), 1095, 1041, and 616 cm^{-1} (ClO_4^-); HR-MS (FAB, pos.) m/z = 559.1770 calcd for $C_{33}H_{31}N_3NiO_2$: 559.1768; Anal. Calcd for $[Ni^{II}(L^{OMe})(CH_3CN)(CH_3OH)](ClO_4)_2\cdot H_2O$ ($C_{36}H_{40}NiCl_2N_4O_{12}$): C, 50.85; H, 4.74; N, 6.59. Found: C, 51.06; H, 4.46; N, 6.51.

$[Ni^{II}(L^{Me})(CH_3CN)(H_2O)](ClO_4)_2$($1^{Me}$). This compound was synthesized in a similar manner using ligand L^{Me} (93.8 mg, 0.2 mmol) instead of L^{OMe} as green powder in 67%. FT-IR (KBr) 3387 cm^{-1} (OH), 1119, 1044, and 625 cm^{-1} (ClO_4^-); HR-MS (FAB, pos.) m/z = 527.1866 calcd for $C_{33}H_{31}N_3Ni$: 527.1871; Anal. Calcd for $[Ni^{II}(L^{Me})(CH_3CN)(H_2O)](ClO_4)_2\cdot H_2O$ ($C_{35}H_{38}NiCl_2N_4O_{10}$): C, 52.27; H, 4.76; N, 6.97. Found: C, 52.10; H, 4.43; N, 6.58.

$[Ni^{II}(L^{Cl})(CH_3CN)(H_2O)](ClO_4)_2$ (1^{Cl}). This compound was synthesized in a similar manner using ligand L^{Cl} (102.8 mg, 0.2 mmol) instead of L^{Me} as green powder in 60%. Single crystals of $\mathbf{1^{Cl}}$ suitable for X-ray crystallographic analysis were obtained by vapor diffusion of ether into a CH_3CN-CH_3OH (1: 1) solution of the complex. FT-IR (KBr) 3426 cm^{-1} (OH), 1122, 1044, and 626 cm^{-1} (ClO_4^-); HR-MS (FAB, pos.) m/z = 567.0756 calcd for $C_{31}H_{25}Cl_2N_3Ni$: 567.0779; Anal. Calcd for $[Ni^{II}(L^{Cl})(CH_3CN)(H_2O)](ClO_4)_2\cdot CH_3CN\cdot H_2O$ ($C_{35}H_{35}NiCl_4N_5O_{10}$): C, 47.44; H, 3.98; N, 7.90. Found: C, 47.17; H, 4.10; N, 7.93.

$[Ni^{II}(L^{NO_2})(CH_3CN)_2(H_2O)](ClO_4)_2$ (1^{NO_2}). This compound was synthesized in a similar manner using ligand L^{NO_2} (106.3 mg, 0.2 mmol) instead of L^{Cl} as green powder in 87%. FT-IR (KBr) 3378 cm^{-1} (OH), 1541 and 1358 cm^{-1} (NO_2^-), 1122, 1044, and 627 cm^{-1} (ClO_4^-); HR-MS (FAB, pos.) m/z = 589.1250 calcd for $C_{31}H_{25}N_5NiO_4$: 589.1260; Anal. Calcd for $[Ni^{II}(L^{NO_2})(CH_3CN)_2(H_2O)](ClO_4)_2\cdot(1/2)H_2O$ ($C_{35}H_{34}NiCl_2N_7O_{13.5}$): C, 46.80; H, 3.82; N, 10.91. Found: C, 46.85; H, 3.95; N, 11.15.

$[Ni^{II}(L^HO)](ClO_4)$ (4^H). An acetone solution (50 mL) of $\mathbf{1^H}$ (75.6 mg, 0.2 mM) was cooled to −90 °C using a dry ice−AcOEt bath. Then, 30% H_2O_2 aqueous solution (0.5 equiv) and Et_3N (1 equiv) were added to the solution. The resulting mixture was stirred for 1 h at −90 °C and then gradually warmed up to room temperature. After stirring for additional 30 min at room temperature, the solvent was removed under reduced pressure to give a brown residue, to which ether (100 mL) was added. The resulting brown powder was precipitated by standing the mixture for several minutes. The supernatant was then removed by decantation, and the remaining green-brown solid was washed with ether three times and dried to give $\mathbf{4^H}$ in 50%. FT-IR (KBr) 1102 and 626 cm^{-1} (ClO_4^-); HR-MS (FAB, pos) 514.1434 calcd for $C_{31}H_{26}N_3NiO$: 514.1429; Anal. Calcd for $[Ni^{II}(L^{OH})](ClO_4)\cdot(1/2)H_2O$ ($C_{31}H_{27}NiCl_1N_3O_{5.5}$): C, 59.70; H, 4.36; N, 6.74. Found: C, 60.08; H, 4.25; N, 6.92. Isotope labeling experiment was performed using $H_2{}^{18}O_2$ instead of $H_2{}^{16}O_2$ by the same method as described above. HRMS m/z = 516.1475 calcd for 516.1472; ($C_{31}H_{26}NiN_3{}^{18}O$).

Product Analysis of Hydroxylated Ligand L^H-OH. After the reaction described above, the reaction mixture was acidified to pH 1 by adding conc. HCl. Removal of the solvent by evaporation gave an oily material, which was dissolved into an NH_3 aqueous solution. The aqueous solution was then extracted with ether (20 mL × 5), and the combined organic layer was dried over Na_2SO_4. After removal of Na_2SO_4 by filtration, evaporation of the solvent gave a yellow material, from which the hydroxylated ligand L^H-OH was isolated as an oily material by silica gel column chromatography (eluent: Hexane/AcOEt = 6: 1). ^1H NMR (400 Hz, $CDCl_3$) δ 3.78 (2 H, s, -CH_2-Ph), 3.89 (2 H, s, -N-CH_2-Py), 3.92 (2 H, s, -N-CH_2-Py), 6.89 (1 H, t, J = 8.0 Hz), 7.04 (1 H, d, J = 8.0 Hz), 7.20−7.25 (1 H, m), 7.27−7.37 (3 H, m), 7.39 (1 H, d, J = 8.0 Hz), 7.43 (1 H, s), 7.46 (4 H, t, J = 6.4 Hz), 7.57 (2 H, t, J = 7.4 Hz), 7.72 (1 H, d, J = 7.6 Hz), 7.74−7.81 (3 H, m), 7.98 (2 H, d, J = 8.0 Hz).; HR-MS (FAB, pos) m/z = 458.2229, calcd for $C_{31}H_{28}ON_3$ 458.2232.

The yield of hydroxylated ligand L^H-OH was determined as 48% based on the Ni(II) starting material by using an integral ratio in the ^1H NMR spectrum between the benzylic proton (-CH_2-) at δ 3.92 of L^H-OH and that of the original ligand L^H at δ 3.96.

Product Analysis of Hydroxylated Ligand L^{Me}-OH. The reaction of $\mathbf{1^{Me}}$ and H_2O_2 was carried out under the same conditions as described for $\mathbf{1^H}$ (see above). The same workup treatment gave a yellow oily material, from which the hydroxylated ligand L^{Me}-OH was isolated as oil by silica gel column chromatography (eluent: Hexane/AcOEt = 5: 1). The detailed ^1H NMR data are presented in Supporting Information, Figure S26; HR-MS (FAB, pos) m/z = 486.2545, calcd for $C_{33}H_{32}ON_3$ 486.2549.

Product Analysis of Hydroxylated Ligand L^{Cl}-OH. The reaction of $\mathbf{1^{Cl}}$ and H_2O_2 was carried out under the same conditions as described for $\mathbf{1^H}$ (see above). The same workup treatment gave a yellow oily material, from which the hydroxylated ligand L^{Cl}-OH was isolated as oil by silica gel column chromatography (eluent: $CHCl_3$). The detailed ^1H NMR data are presented in Supporting Information, Figures S27 and S28; HR-MS (FAB, pos) m/z = 526.1455, calcd for $C_{31}H_{26}ON_3Cl_2$ 526.1453.

X-ray Structure Determination. Single crystals of $\mathbf{1^X}$ (X = H, OMe, Me, Cl, and NO_2) and $\mathbf{4^H}$ suitable for X-ray crystallographic analysis were obtained by vapor diffusion of ether into an CH_3CN-CH_3OH (1:1) solution of the complex (in the case of $\mathbf{4^H}$, acetone solution). Each single crystal was mounted on a glass-fiber. Data of X-ray diffraction were collected by a Rigaku RAXIS-RAPID imaging plate two-dimensional area detector using graphite-monochromated Mo $K\alpha$ radiation (λ = 0.71069 Å). All the crystallographic calculations were performed by using Crystal Structure software package of the Molecular Structure Corporation [Crystal Structure: Crystal Structure Analysis Package version 3.8.1, Molecular Structure Corp. and Rigaku Corp. (2005)]. The structures were solved with SIR92 and refined with CRYSTALS. All non-hydrogen atoms and hydrogen atoms except disordered atoms and C6 and C8 atoms of the substituent on the one pyridyl group in $\mathbf{1^{Me}}$ were refined anisotropically. Hydrogen atoms were attached on the atoms refined anisotropically and refined isotropically. Atomic coordinates, thermal parameters, and intramolecular bond distances and angles of the complexes are deposited in the Supporting Information (CIF file format).

Kinetic Measurements. The reaction of nickel(II) complexes with H_2O_2 was performed in a 1.0 cm path length UV−vis cell that was held in a Unisoku cryostat cell holder USP-203. After an acetone solution containing the nickel(II) complex (0.6 mM) and Et_3N (1 equiv) was kept at a desired temperature for several minutes, H_2O_2 (1 equiv) in acetone was injected into the cell through a septum rubber cap with use of a microsyringe. The reaction was monitored by following an increase of the characteristic absorption band due to the nickel active-oxygen complexes.

Results and Discussion

Characterization of Nickel(II) Starting Materials ($\mathbf{1^X}$; X = OMe, Me, H, Cl, and NO_2). The nickel(II) complexes $\mathbf{1^X}$ were prepared by treating the ligand L^X with

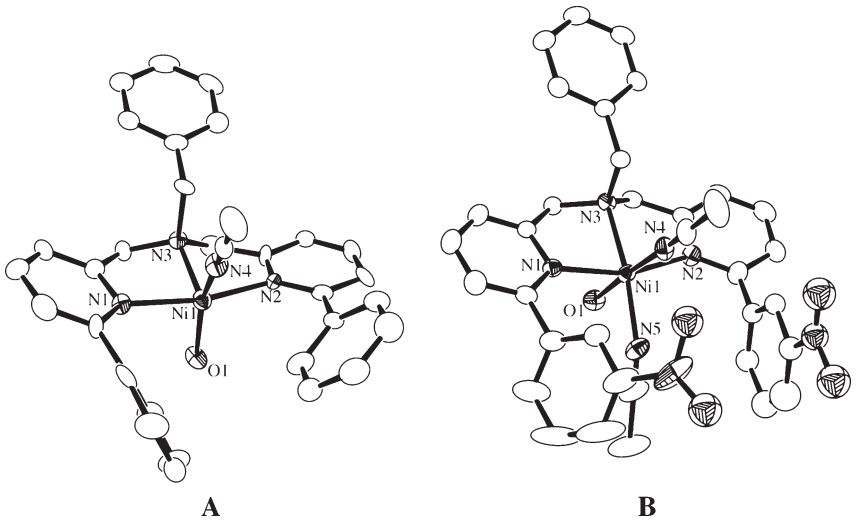

A B

Figure 1. ORTEP drawings of the cationic parts of (A) $[Ni^{II}(L^{H})(CH_3CN)(H_2O)](ClO_4)_2$ ($\mathbf{1^H}$) and (B) $[Ni^{II}(L^{NO_2})(CH_3CN)_2(H_2O)](ClO_4)_2$ ($\mathbf{1^{NO_2}}$) showing 50% probability thermal ellipsoids. The hydrogen atoms are omitted for clarity.

Table 1. Summary of the X-ray Crystallographic Data of Complexes $\mathbf{1^H}$ and $\mathbf{1^{NO_2}}$

	complex $\mathbf{1^H}$	complex $\mathbf{1^{NO_2}}$
formula	$C_{33}H_{29}N_3NiCl_2O_8$	$C_{36}H_{35.5}N_{7.5}NiCl_2O_{13.5}$
formula weight	725.21	918.82
crystal system	monoclinic	monoclinic
space group	*C*2/*c* (No. 15)	*P*2/*a* (No. 13)
a, Å	39.60(3)	17.660(12)
b, Å	10.404(5)	11.152(7)
c, Å	18.200(9)	20.295(11)
α, deg	90	90
β, deg	116.311(19)	98.86(2)
γ, deg	90	90
V, Å^3	6722(6)	3949(4)
Z	8	4
F(000)	2992.00	1896.00
D_{calcd}, g/cm^{-3}	1.433	1.545
T, K	153	153
crystal size, mm	0.20 × 0.15 × 0.10	0.50 × 0.5 × 0.4
μ (Mo*K*α), cm^{-1}	7.903	7.035
$2\theta_{max}$, deg	55.0	54.9
no. of reflns measd	31175	34938
no. of reflns obsd	5430 ([$I > 0.20\sigma I$])	5742 ([$I > 1.50\sigma(I)$])
no. of variables	472	552
R^a	0.0417	0.0577
$R_w{}^b$	0.0776	0.0837
GOF	1.038	0.903

$^a R = \sum||F_o| - |F_c||/\sum|F_o|$. $^b R_w = [\sum w(|F_o| - |F_c|)^2/\sum wF_o^2]^{1/2}$.

$Ni^{II}(ClO_4)_2 \cdot 6H_2O$ in CH_3CN-MeOH (1:1). The crystal structures of $[Ni^{II}(L^{H})(CH_3CN)(H_2O)](ClO_4)_2$ ($\mathbf{1^H}$) and $[Ni^{II}(L^{NO_2})(CH_3CN)_2(H_2O)](ClO_4)_2$ ($\mathbf{1^{NO_2}}$) are shown in Figure 1 as the typical examples. The crystallographic data and the selected bond lengths and angles of those complexes are summarized in Tables 1 and 2, respectively, and those data of other complexes $\mathbf{1^{OMe}}$, $\mathbf{1^{Me}}$, and $\mathbf{1^{Cl}}$ are presented in Supporting Information, Figures S1−S3, Tables S1 and S2. The nickel(II) complex $\mathbf{1^H}$ exhibits a five-coordinate square pyramidal geometry ($\tau = 0.12$),[12] where two pyridine nitrogen atoms N(1) and N(2), oxygen atom O(1) of H_2O, and nitrogen atom N(4) of CH_3CN occupy each corner of the equatorial plane and tertiary amine nitrogen atom N(3) exists at the axial position (Figure 1A). Ni(II) complexes $\mathbf{1^{OMe}}$, $\mathbf{1^{Me}}$, and $\mathbf{1^{Cl}}$ take a similar five coordinate structure involving H_2O (CH_3OH in place of H_2O in $\mathbf{1^{OMe}}$) and CH_3CN as the co-ligands (Supporting Information, Figures S1−S3). On the other hand, $\mathbf{1^{NO_2}}$ shows a six-coordinate octahedral geometry having additional CH_3CN co-ligand (Figure 1B). In this case, one of the aromatic substituents connected to the 6-position of pyridine ring is disordered. The strong electron-withdrawing NO_2 group on the aromatic substituents may reduce the electron-donor ability of pyridine, causing an increase of Lewis acidity of the Ni(II) center. This may enhance the binding ability of the metal ion to the external co-ligands, taking the six-coordinate structure. All of the Ni(II) complexes exhibit several ^{1}H NMR resonances spread over a chemical shift range of ∼60 ppm (Supporting Information, Figures S4−S8), indicating a high-spin ground-state of the complexes ($S = 1$).

Table 2. Selected Bond Lengths (Å) and Angles (deg) of Complexes $\mathbf{1^H}$ and $\mathbf{1^{NO_2}}$

Complex $\mathbf{1^H}$			
Ni(1)−N(1)	2.082(5)	Ni(1)−N(2)	2.061(5)
Ni(1)−N(3)	2.034(5)	Ni(1)−N(4)	2.019(5)
Ni(1)−O(1)	2.027(5)		
N(1)−Ni(1)−N(2)	165.4(2)	N(1)−Ni(1)−N(3)	83.4(2)
N(1)−Ni(1)−N(4)	88.7(2)	N(2)−Ni(1)−N(3)	82.0(2)
N(2)−Ni(1)−N(4)	96.2(2)	N(3)−Ni(1)−N(4)	104.3(2)
O(1)−Ni(1)−N(1)	92.99(19)	O(1)−Ni(1)−N(2)	87.9(2)
O(1)−Ni(1)−N(3)	98.83(19)	O(1)−Ni(1)−N(4)	156.8(2)
Complex $\mathbf{1^{NO_2}}$			
Ni(1)−N(1)	2.155(3)	Ni(1)−N(2)	2.151(3)
Ni(1)−N(3)	2.124(2)	Ni(1)−N(4)	2.062(3)
Ni(1)−N(5)	2.058(3)	Ni(1)−O(1)	2.100(3)
N(1)−Ni(1)−N(2)	161.31(11)	N(1)−Ni(1)−N(3)	80.84(11)
N(1)−Ni(1)−N(4)	93.34(12)	N(1)−Ni(1)−N(5)	96.34(13)
N(2)−Ni(1)−N(3)	80.47(12)	N(2)−Ni(1)−N(4)	88.42(13)
N(2)−Ni(1)−N(5)	102.08(13)	N(3)−Ni(1)−N(4)	95.66(12)
N(3)−Ni(1)−N(5)	169.58(13)	N(4)−Ni(1)−N(5)	94.51(14)
O(1)−Ni(1)−N(1)	89.12(12)	O(1)−Ni(1)−N(2)	89.93(12)
O(1)−Ni(1)−N(3)	86.79(11)	O(1)−Ni(1)−N(4)	176.77(12)
O(1)−Ni(1)−N(5)	83.12(12)		

Reaction of $\mathbf{1^X}$ and H_2O_2. Addition of 1 equiv of H_2O_2 into an acetone solution of the nickel(II) complex $\mathbf{1^H}$

(12) Addison, A. W.; Rao, T. N.; Reedijk, J.; van Rijn, J.; Verschoor, G. C. *J. Chem. Soc., Dalton Trans.* **1984**, 1349–1356.

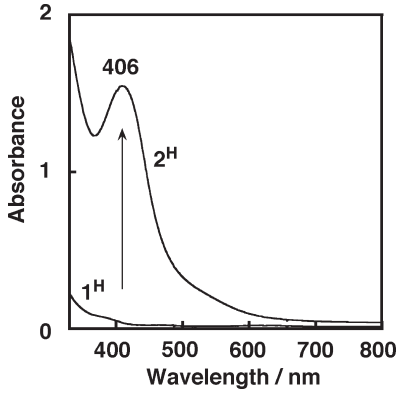

Figure 2. UV−vis spectra of $\mathbf{1^H}$ (0.6 mM) and $\mathbf{2^H}$ generated by the reaction of $\mathbf{1^H}$ and H_2O_2 (0.6 mM) in the presence of NEt_3 (0.6 mM) in acetone at −90 °C.

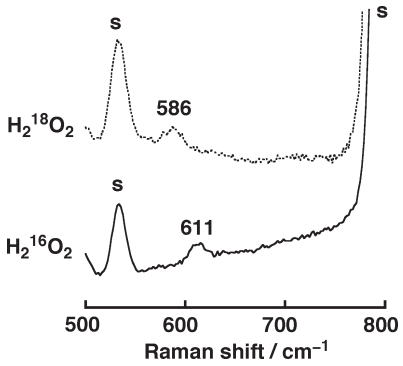

Figure 3. Resonance Raman spectra of the reaction solution of $\mathbf{1^H}$ with $H_2^{16}O_2$ (solid line) and with $H_2^{18}O_2$ (dashed line) obtained with an excitation wavelength of 406.7 nm in acetone at −90 °C: "s" denotes a solvent Raman band.

(0.6 mM) in the presence of triethylamine (1 equiv) at a low temperature resulted in a color change from blue to brown. Figure 2 shows a spectral change of the reaction, where intermediate $\mathbf{2^H}$ exhibiting a characteristic absorption band at 406 nm (ε = 4600 M^{-1} cm^{-1}) readily appears. The characteristic absorption band around 400 nm and its ε value are fairly close to those of the reported bis(μ-oxo)dinickel(III) complexes supported by similar tridentate pyridylalkylamine ligands and have been assigned to oxo-to-metal charge transfer (LMCT) transition.[1b,1e] The resonance Raman spectrum measured at −90 °C with λ_{ex} = 406.7 nm exhibited a characteristic peak at 611 cm^{-1} that shifted to 586 cm^{-1} upon $H_2^{18}O_2$ substitution (Figure 3). The appearance of Raman bands in the 600 cm^{-1} region and their associated isotope shifts ($\Delta\nu$ = 25 cm^{-1}) are also very close to those of the reported bis(μ-oxo)dinickel(III) complexes, where the band has been assigned to a Ni_2O_2 core vibration.[1] In addition, intermediate $\mathbf{2^H}$ was ESR silent. All these spectroscopic characteristics unambiguously suggest that $\mathbf{2^H}$ is a bis(μ-oxo)dinickel(III) complex (**A** in Chart 1), but *not* a HHPP (2-hydroxy-2-hydroperoxypropane) adduct of Ni(II).[13] In support of this, identical UV−vis and resonance Raman spectra were obtained in the reaction of $\mathbf{1^H}$ and H_2O_2 in *propionitrile* at −90 °C, where no acetone molecule is available (Supporting Information,

(13) Instability of $\mathbf{2^H}$ prevents us from getting ESI−MS date even at the low temperature.

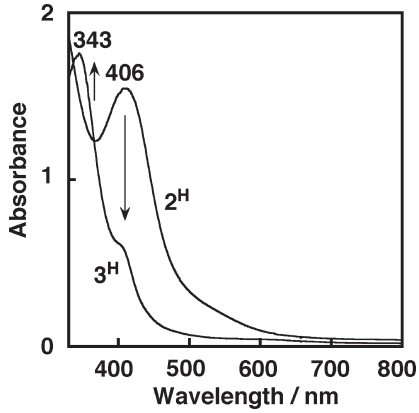

Figure 4. Spectral change for the conversion of $\mathbf{2^H}$ (0.6 mM) to $\mathbf{3^H}$ in acetone at −60 °C.

Figures S10 and S11). Thus, it can be concluded that the reactivity of the Ni(II) complex of L^X toward H_2O_2 is quite different from that of the Cu(II) complex of the same ligand.

Similar UV−vis spectra were obtained in the reactions of $\mathbf{1^{Me}}$, $\mathbf{1^{Cl}}$, and $\mathbf{1^{NO_2}}$ with H_2O_2 under the same experimental conditions (Supporting Information, Figures S12−S14), indicating that similar bis(μ-oxo) dinickel(III) complexes $\mathbf{2^{Me}}$, $\mathbf{2^{Cl}}$, and $\mathbf{2^{NO_2}}$, were also generated in those reactions. It should be noted, however, that the λ_{max} and ε values of those complexes are not exactly identical to each other: λ_{max} = 406 nm (ε = 4600 M^{-1} cm^{-1}) for $\mathbf{2^H}$; 415 nm (3530 M^{-1} cm^{-1}) for $\mathbf{2^{Me}}$; 420 nm (ε = 2590 M^{-1} cm^{-1}) for $\mathbf{2^{Cl}}$; λ_{max} = 413 nm (ε = 3540 M^{-1} cm^{-1}) for $\mathbf{2^{NO_2}}$, suggesting the existence of interaction between the Ni_2O_2 core and the *m*-substituent on the phenyl group of the ligand. In the case of $\mathbf{1^{OMe}}$, on the other hand, the bis(μ-oxo)dinickel(III) complex $\mathbf{2^{OMe}}$ was not accumulated during the course of the reaction because of the fast follow-up reaction as described below.

Aromatic Ligand Hydroxylation from $\mathbf{2^X}$. Bis(μ-oxo) dinickel(III) complex $\mathbf{2^H}$ gradually decomposed, when the temperature of the solution was raised to −60 °C. Figure 4 shows a spectral change for the conversion of $\mathbf{2^H}$ to $\mathbf{3^H}$, where a characteristic absorption band at 343 nm appears with concomitant decrease of the absorption band at 406 nm due to $\mathbf{2^H}$ (the shoulder around 400 nm may be due to a contamination of the final product $\mathbf{4^X}$, see Figure 6). Similar spectral changes were obtained in the case of $\mathbf{2^{Me}}$, $\mathbf{2^{Cl}}$, and $\mathbf{2^{NO_2}}$ as shown in Supporting Information, Figures S15−S17. On the other hand, $\mathbf{3^{OMe}}$ was generated directly from $\mathbf{1^{OMe}}$ without accumulation of the bis(μ-oxo)dinickel(III) intermediate $\mathbf{2^{OMe}}$ even at the lower temperature (−90 °C) (Supporting Information, Figure S18).

The reaction of $\mathbf{2^X}$ to $\mathbf{3^X}$ (X = Me, H, Cl, and NO_2) obeyed first-order kinetics and the first-order rate constants k_{obs} were determined as 5.6 ± 0.09 × 10^{-2} s^{-1}, 1.1 ± 0.001 × 10^{-3} s^{-1}, 7.5 ± 0.12 × 10^{-4} s^{-1}, and 5.2 ± 0.24 × 10^{-4} s^{-1} at −60 °C, respectively, from the plots of $\ln(A - A_\infty)$ versus time (sec). The Hammett analysis using these rate constants and the substituent constants σ^+ gave a ρ value as −1.5 (Supporting Information, Figure S19), suggesting that the reaction involves an electrophilic aromatic substitution mechan-

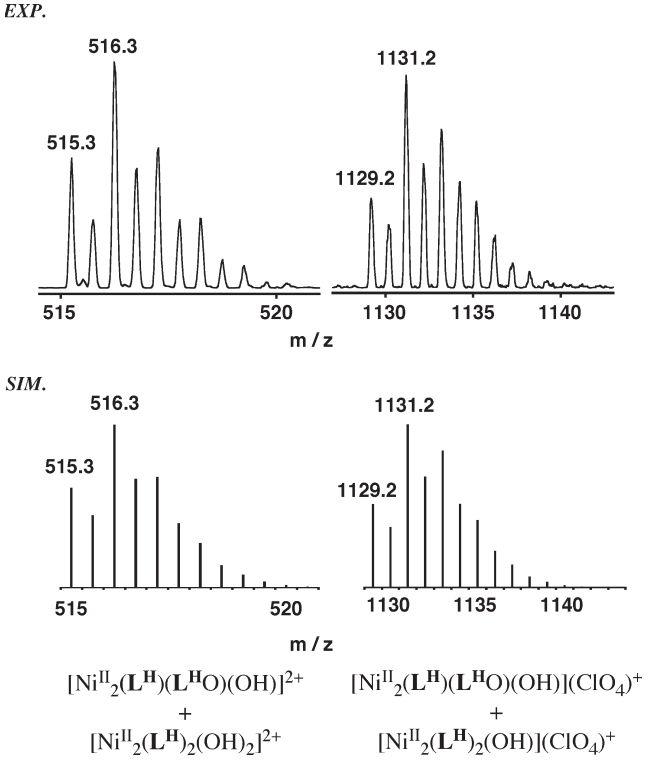

Figure 5. Experimental (top) and calculated (bottom) peak envelopes in the positive-ion electrospray mass spectra of $[Ni^{II}_2(L^H)(L^HO)(OH)]^{2+}$ and $[Ni^{II}_2(L^H)_2(OH)_2]^{2+}$ in a 1:0.6 ratio and $\{[Ni^{II}_2(L^H)(L^HO)(OH)](ClO_4)\}^+$ and $\{[Ni^{II}_2(L^H)_2(OH)_2](ClO_4)\}^+$ in a 1:0.6 ratio.

ism as in the case of the arene hydroxylation reaction by (μ-η^2:η^2-peroxo)dicopper(II) and bis(μ-oxo)dicopper (III) complexes.[14,15]

The reaction was then monitored by ESI-MS at low temperature (Figure 5), where peak clusters at 515.3−520.3 and 1129.2−1141.2 were detected. The former peak cluster could be simulated by assuming the existence of $[Ni^{II}_2(L^H)(L^HO)(OH)]^{2+}$ and $[Ni^{II}_2(L^H)_2(OH)_2]^{2+}$ in a 1:0.6 ratio, where L^HO denotes the deprotonated form of a hydroxylated ligand. Another peak cluster at 1129.2−1141.2 could also be reproduced by adding the simulation spectra of $[Ni^{II}_2(L^H)(L^HO)(OH)](ClO_4)^+$ and $[Ni^{II}_2(L^H)_2(OH)_2](ClO_4)^+$ in a 1:0.6 ratio.

When the temperature of the reaction mixture was raised to room temperature, further spectral change was observed as shown in Figure 6. The final spectrum exhibiting an intense absorption band at 403 nm was identical to the spectrum of $[Ni^{II}(L^HO)](ClO_4)$ ($\mathbf{4^H}$), which was isolated from the final reaction mixture in a 50% yield from a preparative scale (the corresponding spectral changes for ligand hydroxylation of other complexes are shown in Supporting Information, Figures S20−S23). In Figure 7 is shown the crystal structure of

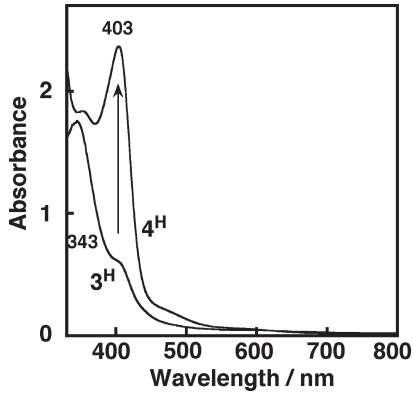

Figure 6. Spectral change for the conversion of $\mathbf{3^H}$ to $\mathbf{4^H}$ in acetone at room temperature.

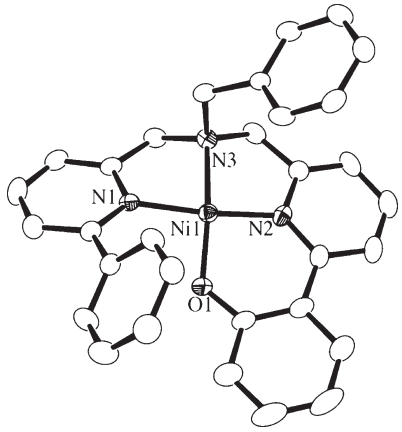

Figure 7. ORTEP drawing of the cationic part of $\mathbf{4^H}$ showing 50% probability thermal ellipsoids. The hydrogen atoms are omitted for clarity.

the isolated $\mathbf{4^H}$ together with the crystallographic data and the selected bond lengths and angles listed in Tables 3 and 4, respectively. As clearly seen in Figure 7, one of the 6-phenyl substituents on the pyridine rings is hydroxylated at its *o*-position, and the nickel(II) center takes a square planar structure with a N_3O donor set.[16] The ESI-MS of final reaction mixture with $H_2{}^{16}O_2$ gave a set of peaks at 514.2 corresponding to $\mathbf{4^H}$ which shifted to 516.3 upon $H_2{}^{18}O_2$ substitution (Supporting Information, Figure S24). The result clearly demonstrated that the oxygen atom introduced into the hydroxylated ligand derived from H_2O_2 used for the generation of $\mathbf{2^H}$.

In the case of *meta*-substituted derivatives ($X \neq H$), the position of hydroxylation could be *ortho* and/or *para* relative to the substituent X. To test this possibility, detailed ^1H NMR analyses were carried out on the modified ligands L^{Me}-OH and L^{Cl}-OH isolated from the preparative scale reactions of $\mathbf{1^{Me}}$ and $\mathbf{1^{Cl}}$ with H_2O_2, respectively (see Experimental Section). In Supporting Information, Figures S26−S28 are shown the detailed ^1H NMR data (chemical shift, multiplicity, coupling constant, 1D NOESY and NOESY correlations) determined by the

(14) (a) Itoh, S.; Kumei, H.; Taki, M.; Nagatomo, S.; Kitagawa, T.; Fukuzumi, S. *J. Am. Chem. Soc.* **2001**, *123*, 6708–6709. (b) Palavicini, S.; Granata, A.; Monzani, E.; Casella, L. *J. Am. Chem. Soc.* **2005**, *127*, 18031–18036. (c) Matsumoto, T.; Furutachi, H.; Kobino, M.; Tomii, M.; Nagatomo, S.; Tosha, T.; Osako, T.; Fujinami, S.; Itoh, S.; Kitagawa, T.; Suzuki, M. *J. Am. Chem. Soc.* **2006**, *128*, 3874–3875.

(15) (a) Holland, P. L.; Rodgers, K. R.; Tolman, W. B. *Angew. Chem., Int. Ed.* **1999**, *38*, 1139–1142. (b) Mirica, L. M.; Vance, M.; Rudd, D. J.; Hedman, B.; Hodgson, K. O; Solomon, E. I.; Stack, T. D. P. *Science* **2005**, *308*, 1890–1892.

(16) Four-coordinate Ni(II) complex $\mathbf{4^H}$ should be diamagnetic (low-spin). However, the compound exhibited several ^1H NMR resonances spread over a chemical shift range from −3 to 30 ppm in CD_3CN (Supporting Information, Figure S9). This may be due to coordination of the solvent molecule(s) to the metal center in the NMR sample solution, which makes the complex with a five or six coordinate structure having a high-spin state.

Table 3. Summary of the X-ray Crystallographic Data of Complex $\mathbf{4^H}$

	complex $\mathbf{4^H}$
formula	$C_{30}H_{27}N_3NiClO_5$
formula weight	603.71
crystal system	monoclinic
space group	$P2_1/n$ (No. 14)
a, Å	13.204(7)
b, Å	11.057(7)
c, Å	18.147(12)
α, deg	90
β, deg	90.24(2)
γ, deg	90
V, Å^3	2649(3)
Z	4
$F(000)$	1252.00
D_{calcd}, g/cm^{-3}	1.513
T, K	153
crystal size, mm	0.15 × 0.15 × 0.10
μ (Mo$K\alpha$), cm^{-1}	8.803
$2\theta_{max}$, deg	54.9
no. of reflns measd	24188
no. of reflns obsd	4227($[I > 0.30\sigma(I)]$)
no. of variables	396
R^a	0.0318
$R_w{}^b$	0.0371
GOF	1.028

$^a R = \sum||F_o| - |F_c||/\sum|F_o|$. $^b R_w = [\sum w(|F_o| - |F_c|)^2/\sum wF_o^2]^{1/2}$.

Table 4. Selected Bond Lengths (Å) and Angles (deg) of Complex $\mathbf{4^H}$

Complex $\mathbf{4^H}$			
Ni(1)−N(1)	1.921(3)	Ni(1)−N(2)	1.854(3)
Ni(1)−N(3)	1.910(3)	Ni(1)−O(1)	1.793(2)
N(1)−Ni(1)−N(2)	172.79(13)	N(1)−Ni(1)−N(3)	84.63(13)
N(2)−Ni(1)−N(3)	88.54(13)	O(1)−Ni(1)−N(1)	91.12(12)
O(1)−Ni(1)−N(2)	95.36(12)	O(1)−Ni(1)−N(3)	171.54(12)

COSY and NOESY measurements (see Experimental Section). As clearly demonstrated by the data, aromatic hydroxylation in $\mathbf{4^{Me}}$ took place selectively at the *para*-position relative to the methyl substituent (X), whereas the hydroxylation occurred at both the *para*- and *ortho*-positions in $\mathbf{4^{Cl}}$ in a 1:0.3 ratio. The higher regio-selectivity in the X = Me system may be due to the steric effect of the substituent. Namely, the larger methyl substituent may prohibit the electrophilic attack to the *ortho*-position by the oxo group in $\mathbf{2^{Me}}$.

Mechanistic Consideration. On the basis of these results, we propose a possible reaction pathway shown in Scheme 2. The reaction of nickel(II) starting material $\mathbf{1^X}$ and H_2O_2 in the presence of triethylamine as the base at a very low temperature (−90 °C) provides the bis(μ-oxo)dinickel(III) complex $\mathbf{2^X}$, the formation of which has been well confirmed by UV−vis and resonance Raman spectra (Figures 2 and 3). This is in sharp contrast to the copper system $Cu^{II}L^X$, where the reaction with H_2O_2 provided the 2-hydroxy-2-hydroperoxypropane (HHPP) adduct in acetone (Scheme 1) and the copper(II)-hydroperoxo complex (L^XCu^{II}−OOH) in propionitrile.[8,9] Thus, the reactivity of the nickel(II) complex $Ni^{II}L^X$ toward H_2O_2 is quite different from that of the copper(II) complex of the same ligand L^X. The reason for such a difference in the H_2O_2-reactivity between these two systems is not clear at present. Accessibility of the higher oxidation state of nickel(III) as compared to copper(III) may enhance the O−O bond cleavage of the initially formed hydroperoxo-adduct. Although formation of such hydroperoxo adduct of Ni(II) (L^XNi^{II}−OOH) could not be

Scheme 2

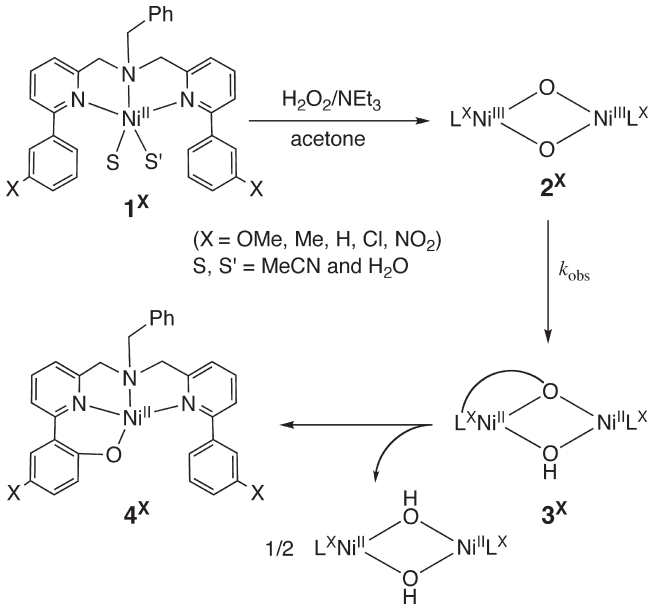

detected during the formation of $\mathbf{2^X}$ from $\mathbf{1^X}$, the titration experiment for the formation of $\mathbf{2^X}$ from $\mathbf{1^X}$ definitely confirmed that the stoichiometry of $\mathbf{1^X}$ to H_2O_2 was 1:1 (Supporting Information, Figure S25). This suggests that L^XNi^{II}−OOH is a precursor of $\mathbf{2^X}$.

At a higher temperature (−60 °C), $\mathbf{2^X}$ gradually decomposes to give (μ-phenoxo)(μ-hydroxo)dinickel(II) complex $[Ni_2^{II}(L^X)(L^XO)(OH)]^{2+}$ ($\mathbf{3^X}$), where one of the ligands L^X was hydroxylated at its 6-phenyl groups to give L^XO. From $\mathbf{3^X}$ mononuclear nickel(II) complex $\mathbf{4^X}$ supported by the modified ligand L^XO is released with concomitant formation of the bis(μ-hydroxo) dinickel(II) product $[Ni_2^{II}(L^X)_2(OH)_2]^{2+}$ at room temperature. $[Ni_2^{II}(L^X)(L^XO)(OH)]^{2+}$ ($\mathbf{3^X}$) and $[Ni_2^{II}(L^X)_2(OH)_2]^{2+}$ were detected by the ESI-MS during the course of the reaction (Figure 5), and the formation of $\mathbf{4^X}$ was definitely confirmed by X-ray crystallographic analysis (Figure 7).

How about the mechanism of the aromatic ligand hydroxylation process ($\mathbf{2^X}$ to $\mathbf{3^X}$)? The observed ρ value (−1.5) in the Hammett analysis (Supporting Information, Figure S19) suggests that the reaction involves an electrophilic aromatic substitution mechanism as demonstrated in the related arene hydroxylation reaction by (μ-η^2:η^2-peroxo)dicopper(II) and bis(μ-oxo)dicopper(III) complexes.[14,15] The higher reactivity of $\mathbf{2^{OMe}}$ having a strong electron-donating substituent (X = OMe), and the observed regio-selectivity of the aromatic hydroxylation reaction (*para*-position relative to the electron-donating substituent X = Me) are consistent with this mechanism. In this case, however, appreciable amount of KIE (kinetic deuterium isotope effect) of 1.8 was obtained using perdeuterated ligand L^H-d_{10} (replacing all protons of the 6-phenyl groups) (Supporting Information, Figure S29). This may indicate that the deprotonation by another oxygen atom of the bis(μ-oxo) core is also involved in the rate-determining step. Thus, we propose that the C−O bond formation and deprotonation occur in a concerted manner as illustrated in Scheme 3. This is the first example of the aromatic hydroxylation reaction by a bis(μ-oxo)dinickel(III) species, providing important

Scheme 3

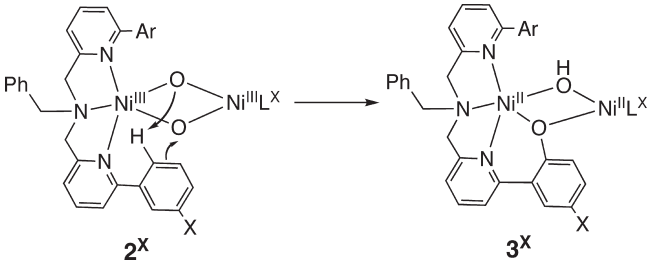

insights into the monooxygenation activity of transition-metal active oxygen complexes.[17]

(17) Honda, K.; Cho, J.; Matsumoto, T.; Roh, J.; Furutachi, H.; Tosha, T.; Kubo, M.; Fujinami, S.; Ogura, T.; Kitagawa, T.; Suzuki, M. *Angew. Chem. Int. Ed.* Advanced Article.

Acknowledgment. The authors thank Dr. Matsumi Doe of Osaka City University for her assistance in obtaining the ^{1}H NMR data of L^{Me}-OH and L^{Cl}-OH. This work was financially supported in part by Grants-in-Aid for Scientific Research on Priority Area (Nos. 19020058, 20036044, and 20037057 for S.I.) and Global Center of Excellence (GCOE) Program ("Picobiology: Life Science at Atomic Level" to T.O.) from MEXT, Japan and by Grants-in-Aid for Scientific Research (No. 20350082 for S.I.) from JSPS, Japan. The authors also thank Asahi Glass Foundation for the financial support and JSPS Research Fellowship (for A.K.).

Supporting Information Available: Further details are given in Figures S1−S29 and in a CIF file. This material is available free of charge via the Internet at http://pubs.acs.org.